Optics Communications 575 (2025) 131278

Contents lists available at ScienceDirect

Optics Communications

journal homepage: www.elsevier.com/locate/optcom

Tunable diode laser absorption spectroscopy for gas detection with a negative curvature anti-resonant hollow-core fiber

Kaiyu Chai, Bo Hu, Zheng Fu, Yukang Li, Kaili Ren, Dongdong Han, Lipeng Zhu, Lei Liang, Yipeng Zheng *

School of Electronic Engineering, Xi'an University of Posts & Telecommunications, Xi'an 710121, China

ARTICLE INFO

Keywords:
All-fiber gas sensing technology
Negative curvature anti-resonant hollow-core fiber
Opto-gas coupling miniature tee
Tunable diode laser absorption spectroscopy

ABSTRACT

In this study, an all-fiber gas sensing technology was proposed, which is based on tunable diode laser absorption spectroscopy in the near infrared. A negative curvature anti-resonant hollow-core fiber was used as the gas chamber and optical channel, and an opto-gas coupling miniature tee was used in the configuration. Down to ppb (parts-per-billion) level noise-equivalent concentration was achieved with a fast-response capability of less than 6 s. The results demonstrated strong long-term stability, with a relative standard deviation of approximately 2.1% over a 12-h period. This approach demonstrates a simple, robust, fast response and compact sensor configuration that contributes to better management of greenhouse gas emissions and environmental pollution.

1. Introduction

Gas detection is critical in environmental monitoring, industrial control, and medical diagnostics. Common detection methods include mass spectrometry, chromatographic analysis, electrochemical methods, and laser spectroscopy [1,2]. Among these, laser spectroscopy stands out for its ability to leverage the unique rotational-vibrational transitions of molecules to detect specific gases with high precision. This technique exploits the laser's high monochromaticity and narrow linewidth, enabling high sensitivity and selectivity in gas detection [3,4]. Traditional free-space laser spectroscopy systems, while offering high resolution and sensitivity, rely on bulky, discrete optical components and free-space gas cells. These systems often require precise alignment and consume significant amounts of gas due to substantial gas exchange volumes [5].

Hollow-core fibers (HCFs) effectively address challenges in gas detection by enabling the coexistence of low-loss propagation modes and gases within the hollow core. This design allows for efficient gas-light interaction over long distances, resulting in high sensitivity, reduced sample gas consumption, and a compact system size [6,7]. Additionally, due to its low gas consumption, the anti-resonant hollow-core fiber (ARHCF) technique shows significant potential in medical breath analysis by minimizing sample requirements and accelerating detection, thereby reducing the burden on patients [8]. The minimal gas loss in this system also enhances the accuracy and sensitivity of gas identification and quantification, making it ideal for chemical analysis [9]. Furthermore, HCFs are well-suited for detecting hazardous gases, such as methane and carbon monoxide, in confined spaces like mines and tunnels, contributing to improved worker safety [10]. By confining both the gas sample and the propagating light within the hollow core, HCFs achieve nearly 100% overlap between the sample and light fields, maximizing detection efficiency [11].

Tunable diode laser absorption spectroscopy (TDLAS) based on an all-fiber system identifies gas components by measuring changes in absorption intensity at specific wavelengths. This method offers advantages such as a wide dynamic range, long-term stability, and low maintenance costs. For instance, Nikodem et al. employed wavelength modulation spectroscopy with an ARHCF with a 63 μm core diameter and a 3.2 m length, achieving a detection limit in the single ppb range and a response time of under 30 s using negative pressure pumping [12]. Jin et al. used a 4 m long ARHCF with a 56 μm inner diameter and a 28 μm capillary diameter, combining photothermal technology and side-punched gas filling to achieve a detection limit in the parts per trillion (ppt) range, with a response time of 44 s and an instability of 0.8% [13]. A modified fiber mating sleeve with side channels enabled a faster response time of 16 s in a 1.2 m ARHCF with a 29.7 μm core diameter [14]. Similarly, Krzempek et al. used an airtight housing to encase a 1.3 m photonic crystal fiber with a 116 μm core diameter, achieving a response time of approximately 10 s under positive pressure [15].

* Corresponding author.
E-mail address: ypzheng@xupt.edu.cn (Y. Zheng).

https://doi.org/10.1016/j.optcom.2024.131278
Received 20 July 2024; Received in revised form 29 October 2024; Accepted 4 November 2024
Available online 5 November 2024

It should be noted that response times are largely influenced by factors such as fiber length, core diameter, inlet pressure and the method of gas injection, making these parameters critical in optimizing system performance.

In this study, we conducted sensitive carbon dioxide (CO_2) detection in a 5-m-long negative curvature anti-resonant hollow-core fiber (NC-ARHCF) using TDLAS at 2.0 μm. A micro-T-type tee-junction valve with high coupling efficiency was designed for gas filling and optical coupling without damaging the waveguide structure. We achieved a response time of approximately 6 s and a noise-equivalent concentration (NEC) at the ppb level. Additionally, we demonstrated that over 12 h, the all-fiber gas CO_2 measurement had a relative standard deviation (RSD) of approximately 2.1%.

2. Negative curvature anti-resonant hollow-core fiber

As depicted in Fig. 1(a), the HCF employed in this study is a NC-ARHCF with a core diameter of 110 μm and a cladding diameter of 320 μm. This core diameter supports a higher gas flow rate under equivalent inlet pressure, effectively increasing the flow velocity within the fiber and reducing the system's response time [16]. The central core is surrounded by multiple anti-resonance tubes with diameters of 40 μm, and the fiber's numerical aperture ranges from 0.02 to 0.03. Light propagation in the NC-ARHCF is primarily governed by the suppression of coupling between the core and cladding modes, rather than by the photonic bandgap mechanism. This allows for efficient single-mode operation and light transmission, even with relatively large core diameters. The structure and size of cladding plays a crucial role in confining the fundamental mode within the hollow air core while suppressing higher-order modes through resonant coupling with the surrounding tube modes [17]. By significantly increasing the loss ratio between fundamental mode and higher-order modes, the NC-ARHCF effectively reduces multimodal interference, which is especially important in large-core fibers. This ensures superior single-mode performance, making the NC-ARHCF highly suitable for applications requiring high precision, stability, and single-mode fiber transmission. As shown in Fig. 1(b), the transmission mode of the NC-ARHCF near the CO_2 absorption peak illustrates that most of the light field energy is effectively confined within the fiber core.

Using a supercontinuum light source with a spectral range of 900 nm–4800 nm, NC-ARHCF was found to have a wide transmission band of 920 nm–4200 nm. In addition, it exhibits significantly high transmission energy and low transmission loss near the CO_2 2000 nm absorption peak region, as shown in Fig. 2 (a) and 2 (b).

3. Experimental setups

The Beer-Lambert absorption law can describe the change in intensity of a beam of known intensity before and after passing through a medium filled with a certain gas [18]. The expression is as follows:

$$I_{out}(\nu) = I_{in}(\nu)\exp[-S(T)\, g(\nu, \nu_0)PCL] \quad (1)$$

Where $I_{in}(\nu)$ is the incident laser intensity, where I_{out} (ν) is the emitted laser intensity, L is the total absorption path long (5 m in our experiment) and g (ν, ν_0) is the normalized linear function of the gas molecular absorption, P is the gas pressure, C is the mole fraction (concentration) of the gas, $S(T)$ represents the temperature-dependent absorption line intensity.

In our experiments, a micro-T-type tee-junction valve was designed for gas filling and optical coupling, as shown in Fig. 3(a). The valve assembly depicted in Fig. 3(a) is constructed using a capillary tube and standard ceramic sleeves, enclosed by heat shrink tubing and sealed with UV glue to prevent gas leakage. As shown in Fig. 3(b), the setup features two transverse interfaces designed for fiber optic connections and a longitudinal interface for gas injection. The standard ceramic sleeves hold the fiber optic connectors in place with a 4 mm gap between them, ensuring co-linear placement between NC-ARHCF and either single-mode fiber (SMF) or multimode fiber (MMF). This alignment helps minimize the propagation of HOM in the NC-ARHCF, reducing fiber fringe formation and improving overall transmission stability [19]. A 1 mm opening left by the heat shrink tubing allows for capillary insertion. The micro-orthogonal capillary can be pressed against the inner wall of the T-junction to enhance the fiber coupling efficiency and reduce light losses. Additionally, eight holes, each 100 μm in diameter, were drilled along the orthogonal tube to mitigate the effects of air turbulence [20].

The experimental setup is illustrated in Fig. 4. A distributed feedback (DFB) laser (Technologies Company, 2004 nm DFB KELD1G5BAAA) with a central wavelength of 2003.4 nm was modulated using a positive sawtooth wave signal at 1 Hz frequency, 0.8 V amplitude, and a 50% duty cycle. The modulated optical signal from the DFB laser was transmitted through a single-mode fiber and collimated at a micro-T-type tee junction with a loss of 0.25 dB, before being coupled into the NC-ARHCF with a loss of 0.035 dB/m (Aunion Tech, FC/PC-FC/PC-ARF8C110/320/420AE–SS–5). The gas was injected vertically into the micro tee using a capillary tube with an inner diameter of 0.3 mm and an outer diameter of 0.8 mm. After the laser light interacted with the gas inside the NC-ARHCF, it was coupled into a 0.5-m-long multi-mode fiber (MMF: Thorlabs, M123L01, core diameter: 200 μm, 0.5 NA), which protected the end face of the NC-ARHCF via the micro-T-type tee junction (shown in Fig. 3(d)). The light was then transmitted to a detector. The detected signal was processed through a 1 kHz low-pass filter (Thorlabs, EF110) before being sent to a data acquisition card (National Instruments, NI 9215) and finally to a computer for further analysis. For gas preparation, the pre-mixed gas was injected into the NC-ARHCF at a pressure of 0.2 MPa and a flow rate of 500 SCCM via the miniature tee structure shown

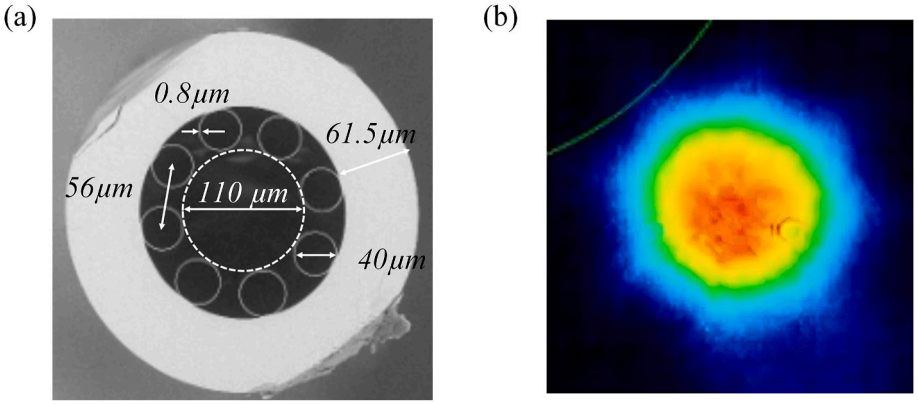

Fig. 1. (a) Cross-section of a 5-m-long NC-ARHCF; (b) Transmission mode at a central of 2250 nm with a bandwidth of 500 nm.

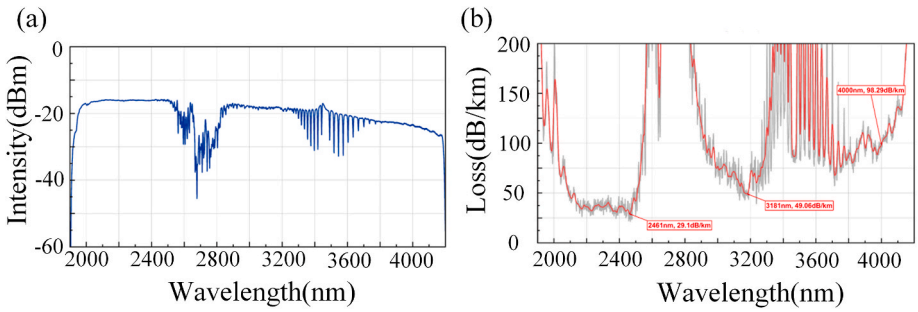

Fig. 2. (a) Transmission spectrum of the negative curvature hollow-core fiber; (b) Loss spectrum of the negative curvature hollow-core fiber.

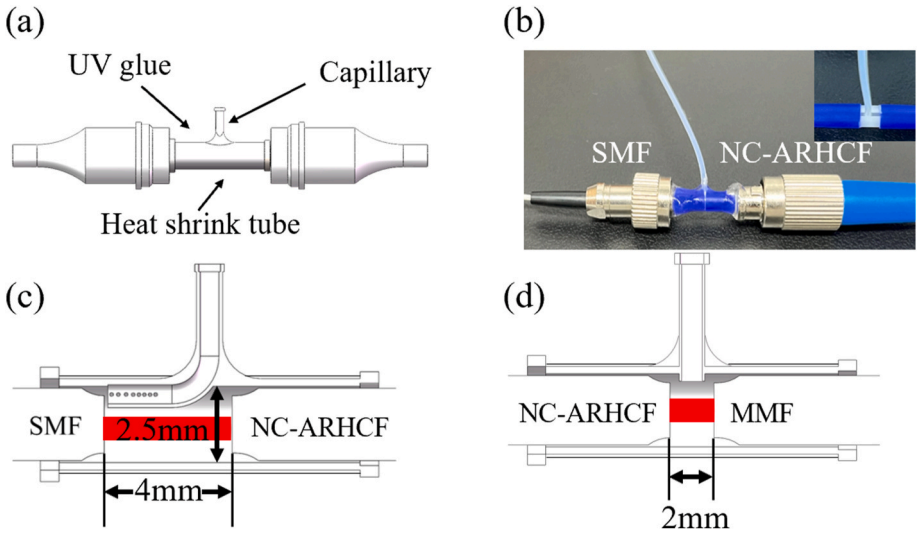

Fig. 3. Micro-T-type tee-junction; (a)Schematic diagram of Micro-T-type tee-junction; (b)Physical diagram of Micro-T-type tee-junction; (c) Connection of SMF to NC-ARHCF; (d) Connection of NC-ARHCF to MMF.

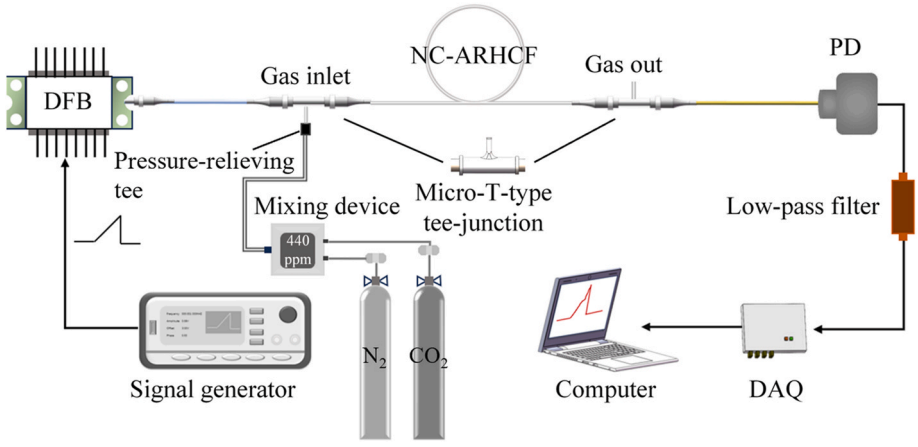

Fig. 4. Experimental setup.

in Fig. 3(c), using a gas mixing device. Additionally, a pressure-relieving tee was incorporated into the gas circuit to manage the high flow rate output from the mixing device.

4. Standardization and Allan deviation

To calibrate the accuracy of the system, experiments were conducted using various concentrations of CO_2. Fig. 5 presents the signal intensity (I_s) for pure nitrogen and CO_2 concentrations of 80 ppm, 440 ppm, and 1000 ppm. It is important to note that with the increase of CO_2 concentration, the absorption intensity increases significantly. In addition, the depeaking fitting method described in Ref. [21] was used. The method involves of removing the absorption portion of the absorption peak and fitting the non-absorption portion with a nine-term equation to obtain a baseline. This method is more accurate than using pure nitrogen as a baseline.

The absorption results were obtained by normalizing the CO_2 absorption signal intensities at 80 ppm, 440 ppm, and 1000 ppm to the

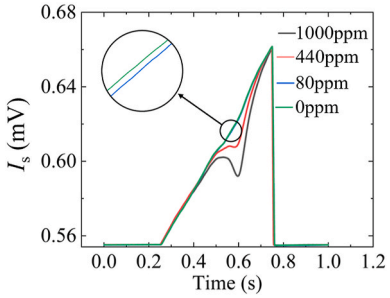

Fig. 5. I_s of CO_2 at different concentrations;.

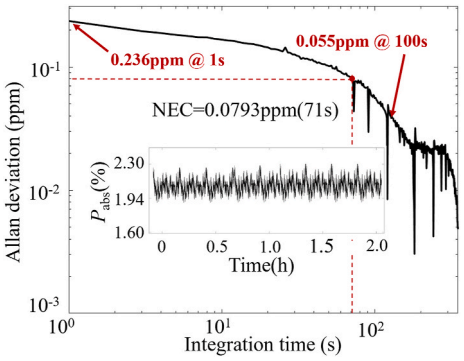

Fig. 7. Time trace (inset) and Allan-Werle plot of absorption noise with 400 ppm CO_2 in the NC-ARHCF.

baseline as shown in Fig. 6(a). Moreover, when NC-ARHCF is filled with nitrogen, a fixed fringe noise appears in the optical signal as show in Fig. 5, which may be caused by the non-ideal output of the DFB laser with external modulation. This fixed noise has been subtracted in the absorption signal. The horizontal axis represents the sampling time, while the vertical axis shows the absorption intensity. The results clearly indicate that the absorption peaks (P_{abs}) increase with rising CO_2 concentration. For system calibration, a standard gas sample with a molar fraction of 1000 ppm (with a 1% uncertainty, supplied commercially) was used. A mixing device configured CO_2 concentrations between 80 ppm and 1000 ppm. Each molar fraction was measured for more than 5 min, and the NC-ARHCF was purged with nitrogen between measurements to prevent interference. Fig. 6(b) shows the linear fitting results, demonstrating that the system exhibits a strong linear response in the 80 ppm–1000 ppm range, with a coefficient of determination close to 1. This indicates that the sensing system performs reliably across a wide concentration range, making it suitable for various practical applications.

The detection limit was theoretically analyzed using the Allan deviation method. The subplot in Fig. 7 shows the P_{abs} over 2 h at a concentration of 400 ppm and a pressure of 0.15 MPa. According to the Allan deviation analysis, the Allan deviation at an integration time of 1 s is 0.236 ppm, indicating the presence of significant noise in the system over short time intervals. However, when the integration time is extended to 100 s, the Allan deviation was reduced by a factor of 4.3, suggesting that the rapid-changing noise can be effectively suppressed with the increase in integration time [22]. Additionally, over an averaging time of 71 s, the NEC for CO_2 reached 0.0793 ppm [23].

5. Stability and faster response time

Fig. 8 shows the long-term stability of the system over a 12-h period based on the Allan deviation optimal average time. Fig. 8(a) shows the overall stability throughout this time, while Fig. 8(b) presents the deviation in I_s over a 5-min interval. Fig. 8(c) highlights the stability of the P_{abs} over 12 h, with an RSD of 2.1%.

The response time was tested by filling NC-ARHCF, via micro-T-type tee-junction, with nitrogen, then 1000 ppm CO_2 in nitrogen. The experimental results demonstrated a response time t_{90} (defined as the time required to reach 90% of the used concentration) was approximately 6 s (as shown in Fig. 9). It takes 15 s to fill the entire NC-ARHCF. The cross-sectional view of the NC-ARHCF is shown in Fig. 1(a), where the white area is quartz wave particles and the black area is gas to be measured. The volume of the gas part of the NC-ARHCF is calculated to be 4.02×10^{-9} m^3. Based on the experimental data, the flow rate within the NC-ARHCF was estimated to be 0.55 SCCM (a pressure-relief tee was utilized to moderate the high flow rate from the mixing device). Furthermore, these response time results suggest that the use of a micro-T-type junction as the gas inlet, which directly interfaces with the hollow-core fiber's end face, can significantly enhance the response speed of the HCF gas sensor.

6. Conclusions

In summary, this study successfully demonstrated the use of NC-ARHCF with a large core diameter in combination with TDLAS for fast-response CO_2 gas concentration monitoring. The integration of a Micro-T Tee junction into the system provided significant advantages in terms of compactness and response time compared to conventional HCF gas injection methods. The system maintained excellent long-term stability, exhibiting an RSD of approximately 2.1% over a 12-h period. These performance characteristics enable the sensor to ensure fast response times while maintaining stable operation over extended durations. Thus, the sensor system is ideal for a wide range of practical applications, including environmental monitoring, industrial process control, and medical diagnostics.

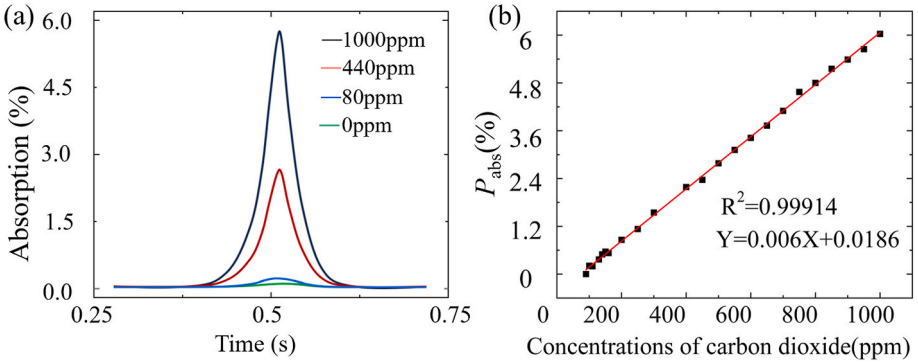

Fig. 6. (a) Absorption profiles extracted from positive sawtooth wave; (b) Linear relationship between CO_2 concentration and the P_{abs} from 80 ppm to 1000 ppm.

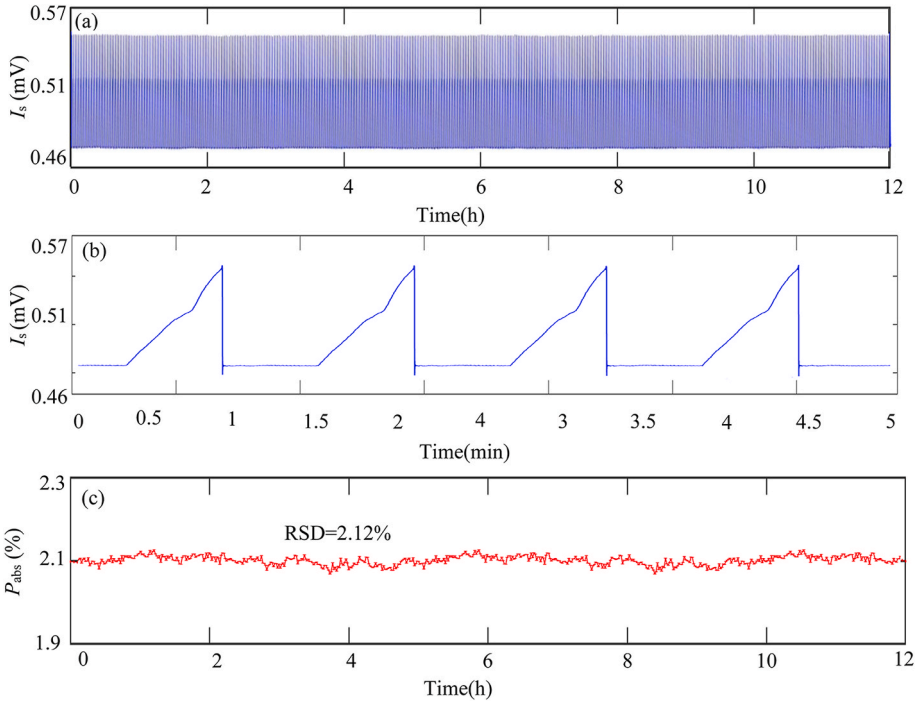

Fig. 8. Results of long-term stability testing; (a) I_s over 12 h; (b) I_s over 5 min; (c) P_{abs} within 12 h.

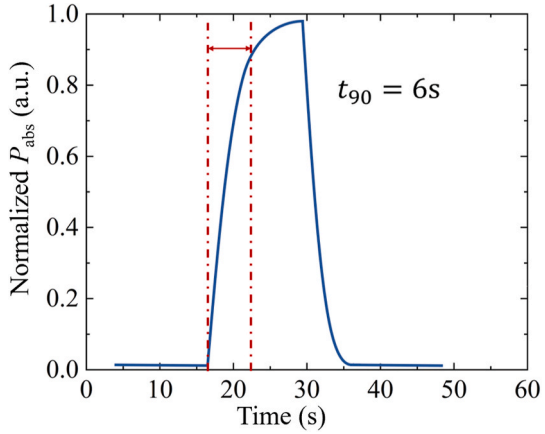

Fig. 9. System response time test results.

CRediT authorship contribution statement

Kaiyu Chai: Writing – review & editing, Writing – original draft, Methodology, Investigation, Formal analysis. **Bo Hu:** Visualization, Software. **Zheng Fu:** Validation. **Yukang Li:** Supervision. **Kaili Ren:** Resources. **Dongdong Han:** Funding acquisition. **Lipeng Zhu:** Resources. **Lei Liang:** Resources. **Yipeng Zheng:** Resources, Project administration, Investigation, Funding acquisition, Formal analysis, Conceptualization.

Declaration of competing interest

The authors declare that they have no known competing financial interests or personal relationships that could have appeared to influence the work reported in this paper.

Acknowledgments

This work was supported by the National Natural Science Foundation of China (Grant No.12304373, 12104368, 62305268); Xi ʾan University of Posts and Telecommunications grad uate Innovation Fund, China project (Grant No. CXJJZL2023012); Natural Science Foundation of Shaanxi Province (Grant No. 2022JM-357). The authors are grateful to Yunzhong Deng for her help with the preparation of some adapters in the experiments.

Data availability

No data was used for the research described in the article.

References

[1] D. Smith, M.J. Mcewan, P. Španěl, et al., Understanding gas phase ion chemistry is the key to reliable selected ion flow tube-mass spectrometry analyses, Anal. Chem. 19 (92) (2020) 12750–12762, https://doi.org/10.1021/acs.analchem.0c03050.
[2] S. Aslani, D. Armstrong, et al., High information spectroscopic detection techniques for gas chromatography, J. Chromatogr. A 1 (1676) (2022) 463255, https://doi.org/10.1016/j.chroma.2022.463255.
[3] B. Henderson, A. Khodabakhsh, M. Metsälä, et al., Laser spectroscopy for breath analysis: towards clinical implementation, Appl. Phys. B 1 (124) (2018) 1–21, https://doi.org/10.1007/s00340-018-7030-x.
[4] S.J. Harris, J. Liisberg, L. Xia, et al., N_2O isotopocule measurements using laser spectroscopy: analyzer characterization and intercomparison, Atmos. Meas. Tech. 5 (13) (2020) 2797–2831, https://doi.org/10.5194/amt-13-2797-2020.
[5] S. Yu, Z. Zhang, H. Xia, et al., Photon-counting distributed free-space spectroscopy, Light Sci. Appl. 1 (10) (2021), https://doi.org/10.1038/s41377-021-00650-2Corpus, 212-212.
[6] M. Nikodem, G. Gomolka, M. Klimczak, et al., Laser absorption spectroscopy at 2 microm inside revolver-type anti-resonant hollow core fiber, Opt Express 25 (27) (2019) 36350–36357, https://doi.org/10.1364/OE.27.014998.
[7] H. Bao, W. Jin, Y. Hong, et al., Phase-modulation-amplifying hollow-core fiber photothermal interferometry for ultrasensitive gas sensing, J. Lightwave Technol. 40 (1) (2022) 313–322, https://doi.org/10.1109/JLT.2021.3120559.
[8] Y. Kudo, S. Kino, Y. Matsuura, Vacuum ultraviolet absorption spectroscopy analysis of breath acetone using a hollow optical fiber gas cell, Sensors 2 (21) (2021) 478, https://doi.org/10.3390/s21020478.
[9] D. Jauregui-Vazquez, P. Lozano-Sotomayor, J. Mejía-Benavides, et al., Binding analysis of functionalized multimode optical-fiber sandwich-like structure with organic polymer and its sensing application for humidity and breath monitoring, Biosensors 11 (9) (2021) 324, https://doi.org/10.3390/bios11090324.
[10] J. Wang, B. Li, W. Wu, et al., Near-infrared dual greenhouse gas sensor based on hollow-core photonic crystal fiber for gas-cell in-situ applications, Sensors 24 (5) (2024) 1670, https://doi.org/10.3390/s24051670.

[11] A. Kumar, P. Malevich, L. Mewes, et al., Transient absorption spectroscopy based on uncompressed hollow core fiber white light proves pre-association between a radical ion photocatalyst and substrate, J. Chem. Phys. 14 (158) (2023) 144201, 10.1063/The Journal of Chemical Physic 5.0142225.
[12] M. Nikodem, G. Gomółka, M. Klimczak, et al., Demonstration of mid-infrared gas sensing using an anti-resonant hollow core fiber and a quantum cascade laser, Opt Express 27 (25) (2019) 36350–36357, https://doi.org/10.1364/OE.27.036350.
[13] P. Zhao, Y. Zhao, H. Bao, et al., Mode-phase-difference photothermal spectroscopy for gas detection with an anti-resonant hollow-core optical fiber, Nat. Commun. 1 (11) (2020) 847, https://doi.org/10.1038/s41467-020-14707-0.
[14] M. Nikodem, G. Gomółka, M. Klimczak, et al., Wavelength modulation spectroscopy of oxygen inside anti-resonant hollow-core fiber-based gas cell, Opt Laser. Technol. 1 (170) (2024) 110323, https://doi.org/10.1016/j.optlastec.2023.110323.
[15] M.L. Nikodem, K. Krzempek, et al., Hollow core fiber-assisted absorption spectroscopy of methane at 3.4um, Opt Express 26 (17) (2018) 21843–21848, https://doi.org/10.1364/OE.26.021843.
[16] M. Zhang, Z. Peng, Q. Yang, et al., A high-precision NO x chemiluminescence sensor of sub-ppb-level based on air-fed ozoniser and flow-restricting capillary, Int. J. Environ. Anal. Chem. 1 (1) (2024) 1–16, https://doi.org/10.1080/03067319.2024.2331599.
[17] G. Casasanta, F. Falcini, R. Garra, et al., Beer–Lambert law in photochemistry: a new approach, J. Photochem. Photobiol. Chem. 1 (432) (2022) 114086, https://doi.org/10.1016/j.jphotochem.2022.114086.
[18] G. Casasanta, F. Falcini, R. Garra, et al., Beer–Lambert law in photochemistry: a new approach, J. Photochem. Photobiol. Chem. 1 (432) (2022) 114086, https://doi.org/10.1016/j.jphotochem.2022.114086.
[19] G. Gomółka, D. Pysz, R. Buczyński, et al., Dual-pass hollow-core fiber gas spectroscopy using a reflective configuration with heterodyne-based signal detection, J. Lightwave Technol. 41 (18) (2023) 6094–6101, https://doi.org/10.1109/JLT.2023.3272308.
[20] A. Elfasakhany, X.S. Bai, et al., Numerical and experimental studies of irregular-shape biomass particle motions in turbulent flows, Engineering Science and Technology, an International Journal 22 (1) (2019) 249–265, https://doi.org/10.1016/j.jestch.2018.10.005.
[21] Xiaorui Zhu, Weiye Lu, Yuzhou Rao, et al., Baseline selection method for CO_2 measurement by TDLAS direct absorption, Optics China 10 (4) (2017) 455–461, https://doi.org/10.3788/CO.20171004.0455.
[22] M. Zhang, Z. Peng, Q. Yang, et al., A high-precision NO x chemiluminescence sensor of sub-ppb-level based on air-fed ozoniser and flow-restricting capillary, Int. J. Environ. Anal. Chem. 1 (1) (2024) 1–16, https://doi.org/10.1080/03067319.2024.2331599.
[23] H. Xu, S. Guerrier, R. Molinari, et al., A Study of the Allan variance for constant-mean nonstationary Processes, IEEE Signal Process. Lett. 24 (8) (2017) 1257–1260, https://doi.org/10.1109/LSP.2017.2722222.